Modeling of Solid–Liquid Fluidization in the Stokes Flow Regime Using Two-Phase Flow Theory

Travis V. Thelen and W. Fred Ramirez
Dept. of Chemical Engineering, University of Colorado, Boulder, CO 80309

Two-phase theory is applied to solid−liquid fluidization in the Stokes flow regime. Because inertial terms can be neglected in the Stokes flow regime, the momentum balances are simplified to an algebraic relation between drag, buoyant, and diffusive forces. The resulting convection-dispersion model is then applied to an experimental expanded-bed adsorption system. Two flows are investigated, namely, step changes in the fluidization velocity and step changes in the fluid properties. Experimental data and model simulations are in excellent agreement for both flow configurations. Furthermore, the two-phase model provides an accurate prediction of the observed time delay in bed expansion for step changes in fluid properties, as well as a mechanistic explanation for its observation.

Introduction

Solid−liquid flows are a common occurrence in the chemical process industries, including such general applications as sedimentation, dispersions, and fluidization, with specific applications in mineral classification, paint technology, expanded-bed adsorption, and fluidized-bed bioreactors, to name a few. Many approaches have been investigated to describe solid−liquid mechanics, including mixture theory (van Deemter and van der Laan, 1961; Hinze, 1962; Zuber, 1964; Müller, 1968; Soo, 1969; Green and Naghdi, 1969; Peddieson, 1974; Kenyon, 1976; Bedford and Drumheller, 1983), flux-based models (Kennedy and Bretton, 1966; Asif et al., 1994; Thelen and Ramirez, 1997), and lumped-parameter models (Slis et al., 1959; Fan et al., 1963; Gibilaro et al., 1984; Poncelet et al., 1990). Of the three approaches, the mixture theory models are the most general and are based on a rigorous fluid-mechanic framework.

In recent years, expanded-bed adsorption (EBA) has received considerable attention for applications in biotechnology (e.g., Batt et al., 1995; Hansson et al., 1994; Dasari et al., 1993; Chase and Draeger, 1992a,b; Draeger and Chase, 1991; Draeger, 1991; Gailliot et al., 1990; Somers et al., 1989; Barthels et al., 1958). Early studies, though, have invariably focused on the adsorption properties of these systems, with little attempt to gain an understanding of their fundamental hydrodynamic properties. An understanding of the hydrodynamic properties of these systems is important in order to provide effective design, scale-up, operation, and control of this purification technique.

Chang and Chase (1996) have recently addressed some of the issues concerning the interactions between important adsorption properties and hydrodynamic properties in EBA. In particular, they have investigated the relative adsorption efficiencies for two modes of operation, namely operation at a fixed-bed height and operation at a fixed flow rate. Chang and Chase (1996) contend that operation at a fixed bed height is most efficient. The latter mode of operation requires a method of control, likely model-based due to the complexity of the system.

A number of articles have been presented on the modeling of bed-height dynamics of solid−liquid fluidized beds (Slis et al., 1959; Fan et al., 1963; Gibilaro et al., 1984; Poncelet et al., 1990; Asif et al., 1994; Thelen and Ramirez, 1997); however, these articles have only addressed the bed-height dynamics for changes in the fluidization velocity. As discussed by DeLuca et al. (1994), the characteristics of the bed-height response due to changes in the fluidization velocity and that due to changes in the fluid properties differ markedly. In the case of the latter, there is a significant time delay before the bed responds to changes in the fluid properties. Currently, there are no suitable models for prediction of bed-height transients due to changes in the physical properties of the fluidizing liquid.

Correspondence concerning this article should be addressed to W. F. Ramirez.

In this article, the application of the two-phase flow equations for solid–liquid fluidization is presented in two parts. The first part discusses the theoretical framework of two-phase flow theory and presents the derivation of governing equations for solid–liquid fluidization in the Stokes regime. The derivation of the governing equations proceeds from a specific rather than general viewpoint by taking advantage of limiting assumptions consistent with the Stokes flow conditions in order to simplify the two-phase flow equations. Simplified models based upon the infinite- and zero-dispersion limits are also derived. The second part of the article presents a detailed experimental investigation of solid–liquid fluidization, as applied to the bed-expansion/contraction characteristics of an EBA process. A comparison between experimental and simulation results is presented for two flow configurations. The first considers changes in the fluidization velocity; the second looks at changes in the fluid properties.

Theory

This section develops the governing equations for solid–liquid fluidization, where the inertial effects can be neglected. That is, the analysis is restricted to the Stokes regime, as defined by a particle Reynolds number less than unity

$$Re_p = \frac{v_t d_p \rho_f^*}{\mu} < 1, \tag{1}$$

where v_t is the Stokes settling velocity; d_p is the particle diameter; ρ_f^* is the fluid density; and μ is the fluid viscosity. The Stokes settling velocity at infinite dilution v_t is written as

$$v_t = \frac{2r_p^2(\rho_p^* - \rho_f^*)g}{9\mu}, \tag{2}$$

where ρ_p^* is the particle density. However, Coulson et al. (1991) have shown that the modified particle Reynolds number is more applicable for fluidized systems:

$$Re_{p_m} = \frac{v_o d_p \rho_f^*}{\mu(1-\phi)}, \tag{3}$$

where v_o is the superficial fluidization velocity and ϕ is the particle-phase fraction.

General two-phase model

We begin our analysis by writing the differential forms for the continuity equations. The fluid-phase and solid-phase continuity equations, respectively, are written as

$$\frac{\partial \rho_f}{\partial t} + \nabla\cdot(\rho_f \boldsymbol{v}_f) = 0 \tag{4}$$

$$\frac{\partial \rho_p}{\partial t} + \nabla\cdot(\rho_p \boldsymbol{v}_p) = 0, \tag{5}$$

where ρ_f and ρ_p are the in-suspension densities, and $\boldsymbol{v}_f$ and $\boldsymbol{v}_p$ are the local fluid and particle velocities, respectively. The in-suspension densities ρ_f and ρ_p are related to the intrinsic densities of the fluid and solid as follows

$$\rho_f = \epsilon\rho_f^* \tag{6}$$

$$\rho_p = \phi\rho_p^*, \tag{7}$$

where ϵ is the fluid-phase fraction and ϕ is the solid-phase fraction. At any point in the mixture, the phase fractions for the liquid and solid sum to unity.

$$\epsilon + \phi = 1. \tag{8}$$

The linear momentum equations for the fluid and solid phases, respectively, are written as

$$\rho_f\left(\frac{\partial \boldsymbol{v}_f}{\partial t} + \boldsymbol{v}_f\cdot\nabla\boldsymbol{v}_f\right) = \Sigma F_f \tag{9}$$

$$\rho_p\left(\frac{\partial \boldsymbol{v}_p}{\partial t} + \boldsymbol{v}_p\cdot\nabla\boldsymbol{v}_p\right) = \Sigma F_p \tag{10}$$

where ΣF_f and ΣF_p are the forces acting on the fluid and particle phases, respectively. These forces may include stress forces, turbulent forces, gravitational forces, and electrostatic forces, among others.

In order to solve the system (Eqs. 4–10), constitutive relationships must be developed for the fluid and solid forces. The approach taken in the two-phase flow literature (e.g., Bedford and Drumheller, 1983) is to pose general forms for the constitutive equations. Here, we take a different approach and postulate constitutive equations specific to the problem of interest. That is, we take advantage of knowledge about the problem in order to simplify the governing equations.

Stokesian two-phase model

Under the conditions of Stokes flow, the inertial or acceleration terms can be neglected in the linear momentum balances (e.g., Gibilaro et al., 1984), hence Eqs. 9 and 10 are simplified as

$$\Sigma F_f = 0 \tag{11}$$

$$\Sigma F_p = 0. \tag{12}$$

It is postulated that there are three important forces to consider, namely the drag force, the gravitational force, and a diffusive force.

For solid–liquid systems, there is general acceptance that the particles are individually supported by the fluid (Richardson and Zaki, 1954). As such, under steady-state conditions, the drag force on an individual particle is balanced by its buoyant force. The steady-state drag force exerted on a particle by the fluid can be written as (Lamb, 1932)

$$F_d = \frac{6\pi\mu r_p v_o}{f_1(\phi)} \tag{13}$$

where r_p is the particle radius and $f_1(\phi)$ is the hindered settling function (Davis, 1995). If Eq. 13 is written in terms of the velocity of the fluid relative to the sphere (i.e., $v_r = v_f - v_p$), as it is in Stokes (1901) original work, the drag force is expressed as

$$F_d = \frac{6\pi\mu r_p v_r}{f_2(\phi)}, \tag{14}$$

which, for steady-state conditions (i.e., $v_p = 0$), is equivalent to

$$F_d = \frac{6\pi\mu r_p v_f}{f_2(\phi)}. \tag{15}$$

The hindered settling functions $f_1(\phi)$ and $f_2(\phi)$ are related as follows

$$f_2(\phi) = \frac{f_1(\phi)}{1-\phi} = \frac{f_1(\phi)}{\epsilon}. \tag{16}$$

Many forms have been proposed for the hindered settling function $f_1(\phi)$ (e.g., Davis, 1995; Garside and Al-Dibouni, 1977; Barnea and Mizrahi, 1973), but that proposed by Richardson and Zaki (1954) seems to be favored in the literature (Davis, 1995). The Richardson–Zaki hindered settling function is

$$f_1(\phi) = (1-\phi)^n, \tag{17}$$

where n is an empirical parameter.

The buoyant force on an individual particle is given by (Lamb, 1945)

$$F_b = \frac{4\pi r_p^3(\rho_p^* - \rho_f^*)g}{3}, \tag{18}$$

where g is the gravitational constant. At steady state, the drag (Eq. 13) and buoyant (Eq. 18) forces are balanced, thus

$$\frac{v_o}{v_t} = f_1(\phi). \tag{19}$$

Assuming the Richardson–Zaki correlation is applicable gives

$$\frac{v_o}{v_t} = (1-\phi)^n. \tag{20}$$

Equation 20 is valid for steady-state conditions. For the case where the solid velocity is not zero, the equivalent expression is given by

$$\frac{v_r}{v_t} = (1-\phi)^{n-1}, \tag{21}$$

which is a balance of the dynamic drag force (Eq. 14) and the buoyant force (Eq. 18).

The parameters, v_t and n, can be determined either experimentally or from theoretical considerations. From steady-state expansion data, a log-log plot of fluidization velocity vs. void fraction can be used to regress the parameters. Davis and Birdsell (1988) have shown from experimental data and theoretical arguments that a Richardson–Zaki exponent of $n = 5.0 \pm 0.1$ is typical for the Stokes regime. The Stokes velocity can be determined by substitution of measured values of the physical properties into Eq. 2. However, as noted by Davis (1995), it is difficult to measure the particle diameter more accurately than within a few percent. As this quantity is squared, the resulting error can be greater than 10%.

Dispersion is also an important factor. Truesdell (1962) has argued that diffusion (dispersion), being a change of motion, arises from forces. The motions produced by dispersion forces must conform to the principle of linear momentum. A dispersion velocity can be written as

$$v_d = \frac{-D_p \nabla \rho_p}{\rho_p}, \tag{22}$$

which is a generalization of Fick's law (Truesdell, 1962).

Now, the force balance on the particles is expressed as

$$F_d + F_{\text{disp}} + F_b = 0, \tag{23}$$

where the drag force is given by Eq. 14, the buoyant force by Eq. 18, and the dispersion force by

$$F_{\text{disp}} = \frac{6\pi\mu r_p}{f_2(\phi)} v_d. \tag{24}$$

Since the momentum equations (Eqs. 9–10) are expressed on a per unit volume basis, we divide through by the buoyant mass, m_b, and multiply through by the solid-phase density, ρ_p, in order to express Eq. 23 on a per unit volume basis:

$$\Sigma F_p = \frac{\rho_p}{m_b}\frac{6\pi\mu r_p}{f_2(\phi)}(v_f - v_p) - \frac{D_p}{m_b}\frac{6\pi\mu r_p}{f_2(\phi)}\frac{\partial \rho_p}{\partial z} - \rho_p g = 0, \tag{25}$$

where one-dimensional axial flow is assumed and the buoyant mass is defined as

$$m_b = \frac{4\pi r_p^3(\rho_p^* - \rho_f^*)g}{3}. \tag{26}$$

Substitution of Eq. 7 into Eq. 25 and rearrangement gives

$$\phi(v_f - v_p) - D_p\frac{\partial \phi}{\partial z} - \phi\frac{f_2(\phi) m_b g}{6\pi\mu r_p} = 0. \tag{27}$$

Noting that $(m_b g)/(6\pi\mu r_p) = v_t$, and assuming that the hindered settling function is given by the Richardson–Zaki ex-

pression, Eq. 27 is written as

$$\phi(v_f - v_p) - D_p\frac{\partial\phi}{\partial z} - \phi v_t(1-\phi)^{n-1} = 0. \qquad (28)$$

Now, the continuity equations are utilized to obtain a relationship between the fluid velocity, v_f, and the particle velocity, v_p. It can be shown that the two velocities are related as (see Appendix B, for derivation)

$$v_f = \frac{v_o}{\epsilon} - \frac{\phi}{\epsilon}v_p = \frac{v_o}{1-\phi} - \frac{\phi}{1-\phi}v_p. \qquad (29)$$

Substitution of Eq. 85 into Eq. 28 yields, upon rearrangement, the expression

$$\phi v_p = \phi v_o - \phi v_t(1-\phi)^n - (1-\phi)D_p\frac{\partial\phi}{\partial z}. \qquad (30)$$

The relationship (Eq. 30) is substituted into the solid-phase continuity equation (Eq. 5), giving

$$\frac{\partial\phi}{\partial t} = -\frac{\partial\left[\phi v_o - \phi v_t(1-\phi)^n - (1-\phi)D_p\dfrac{\partial\phi}{\partial z}\right]}{\partial z}. \qquad (31)$$

If v_s is now defined as

$$v_s \equiv v_o - v_t(1-\phi)^n, \qquad (32)$$

then

$$\frac{\partial\phi}{\partial t} = -\frac{\partial\left[\phi v_s - (1-\phi)D_p\dfrac{\partial\phi}{\partial z}\right]}{\partial z}. \qquad (33)$$

Equation 33 is the governing convection–dispersion model. This analysis provides a link between two-phase modeling and flux-based modeling.

Boundary conditions of the Dankwerts type are assumed, namely

$$\phi v_s - (1-\phi)D_p\frac{\partial\phi}{\partial z} = 0 \qquad @ \quad z = 0 \qquad (34)$$

$$\phi v_s - (1-\phi)D_p\frac{\partial\phi}{\partial z} = \phi\frac{dh}{dt} \qquad @ \quad z = h, \qquad (35)$$

where dh/dt is the bed-height velocity. The system (Eqs. 33–35) is a nonlinear PDE, two-point boundary value problem with a nonstationary upper boundary.

Numerical solution

For a numerical solution of the moving boundary-value problem, the front-fixing technique of Landau (1950) and Crank (1984) is adopted. This technique is discussed briefly. A spatial transformation of the form

$$\zeta = \frac{z}{h(t)} \qquad (36)$$

is posed, where the temporal dependence of h is expressed formally. With this transformation, the spatial partial derivatives are written as

$$\frac{\partial\phi}{\partial z} = \frac{1}{h(t)}\frac{\partial\phi}{\partial\zeta} \qquad (37)$$

$$\frac{\partial^2\phi}{\partial z^2} = \frac{1}{h^2(t)}\frac{\partial^2\phi}{\partial\zeta^2}, \qquad (38)$$

and the temporal partial derivative is as follows

$$\left.\frac{\partial\phi}{\partial t}\right|_z = \frac{\partial\phi}{\partial\zeta}\frac{\partial\zeta}{\partial t} + \left.\frac{\partial\phi}{\partial t}\right|_\zeta = \left.\frac{\partial\phi}{\partial t}\right|_\zeta - \frac{\zeta}{h(t)}\frac{dh}{dt}\frac{\partial\phi}{\partial\zeta}. \qquad (39)$$

The transformed partial differential equation was solved by the method of lines. Second-order correct and centered finite difference approximations were used for the spatial derivatives.

The second part of the article is now presented, where an experimental investigation of solid–liquid fluidization, as applied to the bed-expansion/contraction characteristics of an EBA process, is discussed. A comparison between experimental and simulation results is presented for two flow configurations. The first considers changes in the fluidization velocity; the second looks at changes in the fluid properties. The simulation results are based upon solution of Eqs. 33–39 for the given flow configuration.

Fluid Flow-Rate Change

We consider the following problem. A bed of spherical particles of radius r_p and density ρ_p^* is initially fluidized by a fluid of viscosity μ and density ρ_f^* at a superficial velocity v_1. At steady state under these conditions, the solid fraction ϕ_1 is determined from

$$\frac{v_1}{v_t} = f_1(\phi_1), \qquad (40)$$

where the terminal settling velocity of a single particle in the Stokes flow regime is

$$v_t = \frac{2r_p^2(\rho_p^* - \rho_f^*)g}{9\mu}, \qquad (41)$$

and the hindered settling function is given by the Richardson–Zaki expression

$$f_1(\phi_1) = (1-\phi_1)^n. \qquad (42)$$

The steady-state height of the bed under these conditions is

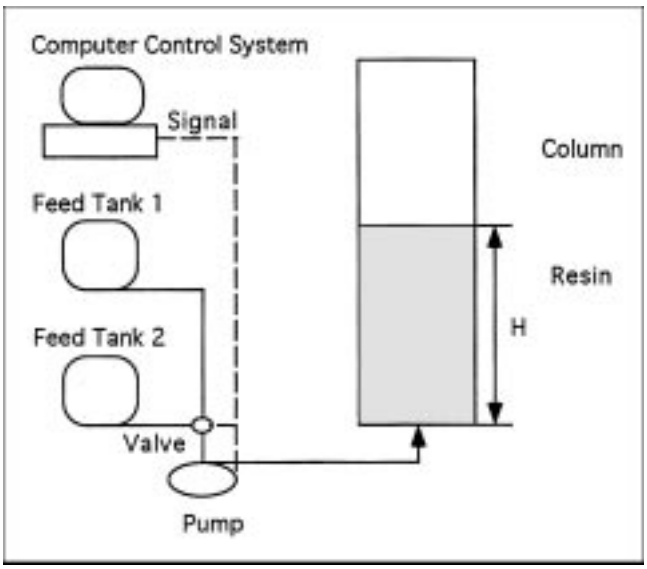

Figure 1. Experimental system.

determined from a particle mass balance

$$h_1 = \frac{\phi_s h_s}{\phi_1}, \tag{43}$$

where ϕ_s and h_s are the solid fraction and height of the settled bed, respectively, before fluidization.

Now, suppose that the fluid entering the bottom of the bed experiences a step change in the fluidization velocity at $t = 0$, so that the bed adjusts to a new steady state given by Eqs. 40–43, but with the subscript 2 (for the new flow conditions) replacing 1. The question to be addressed is how the transient occurs as the bed moves to the new steady state. The two-phase model (Eqs. 33–39) is applied in order to address this question. Additionally, simplified models derived from zero-dispersion and infinite-dispersion limits are discussed. These simplified models provide further insight into the mechanics of the problem.

Experimental system

A STREAMLINE 50 column (5 cm ID) was used in the fluidization studies with STREAMLINE DEAE absorbent (Pharmacia Biotech). The resin has a mean diameter of 200 μm and a mean density of 1.2 g/cm^3. The column and required ancillary equipment are shown in Figure 1. Feedstock was delivered to the column by means of a computer-controlled peristaltic pump (Cole-Parmer). A 20% aqueous ethanol solution with an approximate density of 0.98 g/cm^3 and a viscosity of 0.011 g/cm·s at 25°C was used to fluidize the resin.

The bed was considered to be in a stable state of fluidization if channeling was observed to be minimal in the lower region of the column. The steady-state bed height was recorded for a range of flow rates. The Richardson–Zaki parameters, n and v_t, were determined from linear regression of log-log plots of v_o vs. ϵ. The Stokes settling velocity was also determined using Eq. 2 and measured properties. The regressed and theoretical Stokes values differ considerably, with values of 0.17 ± 0.01 cm/s and 0.44 ± 0.13 cm/s, respectively. The regressed value for the Richardson–Zaki exponent is 4.31.

Models for flow-rate change

In this subsection, three models are presented to address the question of how the transient occurs as the bed moves to a new steady state for a step change in fluidization velocity. The first model is based upon the limiting condition of zero dispersion; the second model is based upon the limiting condition of infinite dispersion; the third model is the two-phase model (Eqs. 33–39).

Zero-Dispersion Limits. Following a change in the fluidization velocity, the void fraction changes progressively from the distributor upwards, until such time that the bed reaches the new steady-state condition. This observation was first made by Slis et al. (1959). A simple mechanistic description of how this transient occurs is presented. The explanation assumes zero dispersion and parallels that presented by Gibilaro et al. (1984); however, the explanations differ in approach.

First, consider the case where the step change involves an increase in the fluidization velocity and the result is an expansion of the bed. Figure 2 shows the steady-state condi-

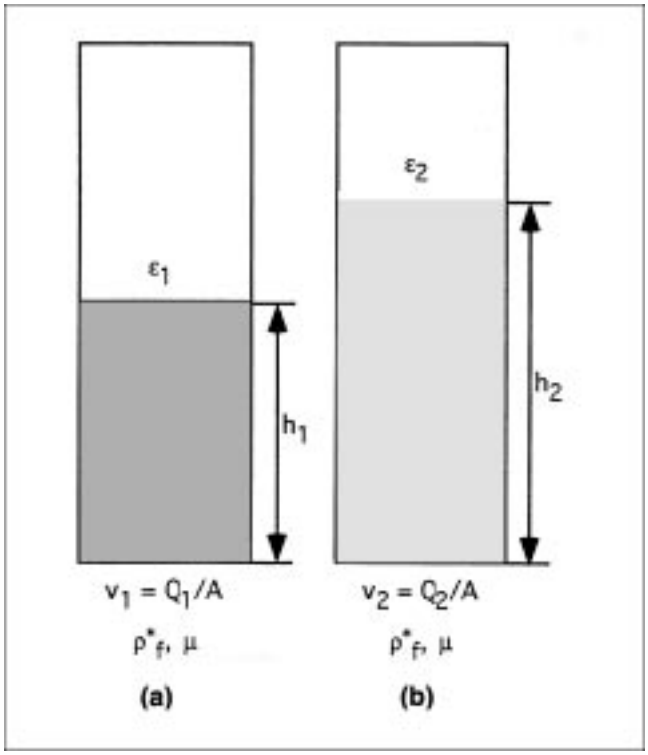

Figure 2. Fluidized bed both before (a) and after (b) a step increase in flow rate ($\epsilon_1 < \epsilon_2$); for the case of a step decrease in flow rate $h_1 > h_2$ and $\epsilon_1 > \epsilon_2$.

tions both before and after the step increase in fluidization velocity.

After the increase in the fluidization velocity from v_1 to v_2, all of the particles are lifted upwards because the superficial velocity now exceeds the settling velocity, that is

$$v_2 > v_1 = v_t f_1(\phi_1). \tag{44}$$

If the bed were to simply rise as a plug, with the void fraction remaining at ϵ_1, this would create a growing layer of clear fluid beneath the rising plug. However, a concentrated region of particles above clear fluid is unstable, and so we expect that particles fall away from the bottom of the rising concentrated region into the less concentrated region below (unless there are strong cohesive forces between the particles that hold the plug together). It is expected that the growing lower region near the bottom of the bed is at a void fraction of ϵ_2, so that the particles on average are stationary in this region due to a balance of buoyancy and drag forces. Thus the bed expands such that there is an interface below which the particles are at a void fraction ϵ_2 and above which the particles are at a void fraction ϵ_1. Figure 3 shows this process. In Figure 3, $h_b(t)$ is the bed height and $h_i(t)$ is the height of the idealized interface. The analogous arguments are valid for the case where the fluidization velocity is reduced, though in this case

$$v_2 < v_1 = v_t f_1(\phi_1), \tag{45}$$

and the bed is expected to decrease in height. Figure 4 shows the void fraction discontinuity for a step decrease in the fluidization velocity.

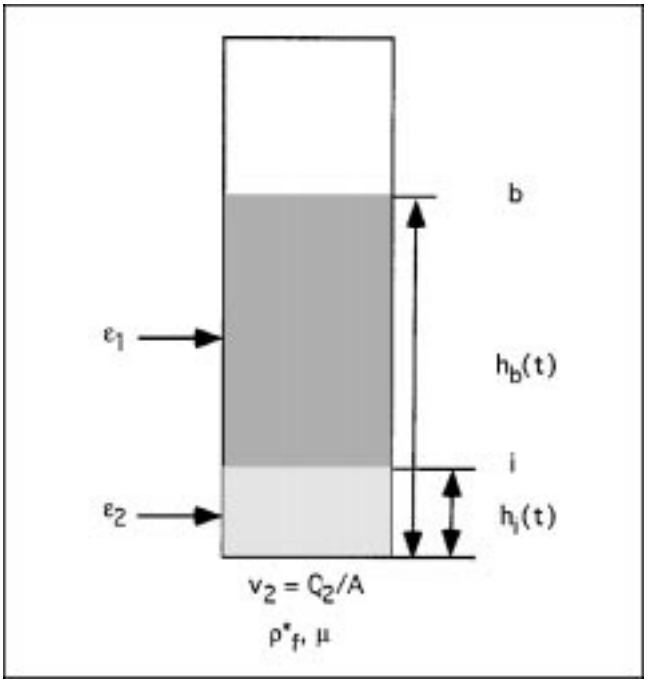

Figure 3. Idealized bed expansion due to a step increase in flow rate for the limit of zero dispersion ($\epsilon_1 < \epsilon_2$).

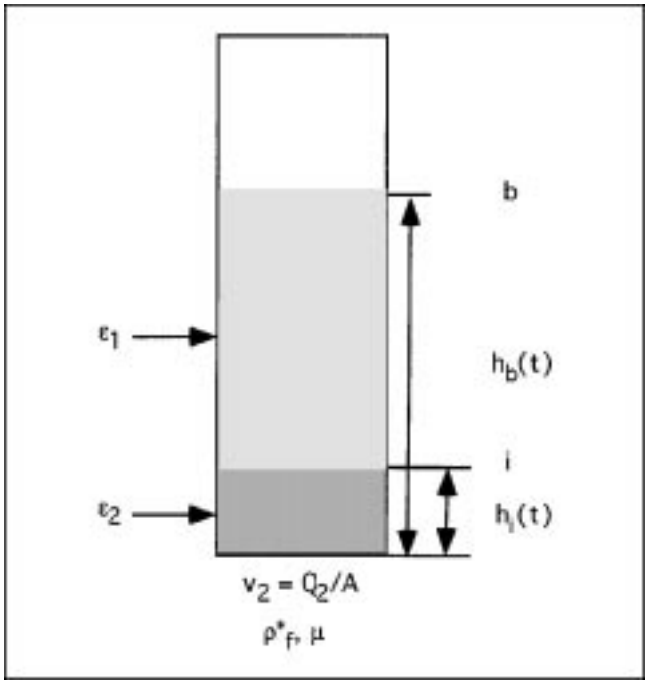

Figure 4. Idealized bed contraction due to a step decrease in flow rate for the limit of zero dispersion ($\epsilon_1 > \epsilon_2$).

The velocities of the interfaces dh_i/dt and dh_b/dt can be determined from mass balances on the solid phase. Across the i interface, the mass flux of solid entering is equal to the mass flux of solid leaving

$$\phi_2\left(\frac{dh_i}{dt} - v_{s,2}\right) = \phi_1\left(\frac{dh_i}{dt} - v_{s,1}\right), \tag{46}$$

where $v_{s,2}$ [the subscripts on $v_{s,\beta}$ have the following meaning: s indicates the solid and is used to denote the particle velocity in the absence of dispersion forces, and β indicates the local void fraction ($v_{s,\beta} = v_2 - v_t(1-\phi_\beta)^n$] is the velocity of the particles below the interface, $v_{s,1}$ is the velocity of the particles above the interface, and dh_i/dt is the velocity of the i interface. The particle velocities are defined as follows (see Appendix A for a derivation of the particle velocity)

$$v_{s,1} = v_2 - v_t(1-\phi_1)^n = v_2 - v_1 \tag{47}$$

$$v_{s,2} = v_2 - v_t(1-\phi_2)^n = v_2 - v_2 = 0. \tag{48}$$

Equation 46 can be rearranged in terms of the interface velocity

$$\frac{dh_i}{dt} = \frac{\phi_1}{\phi_1 - \phi_2} v_{s,1} - \frac{\phi_1}{\phi_1 - \phi_2}(v_2 - v_1). \tag{49}$$

Likewise, across the b interface, the mass flux of solid entering is equal to the mass flux of solid leaving

$$\phi_1\left(\frac{dh_b}{dt} - v_{s,1}\right) = 0, \tag{50}$$

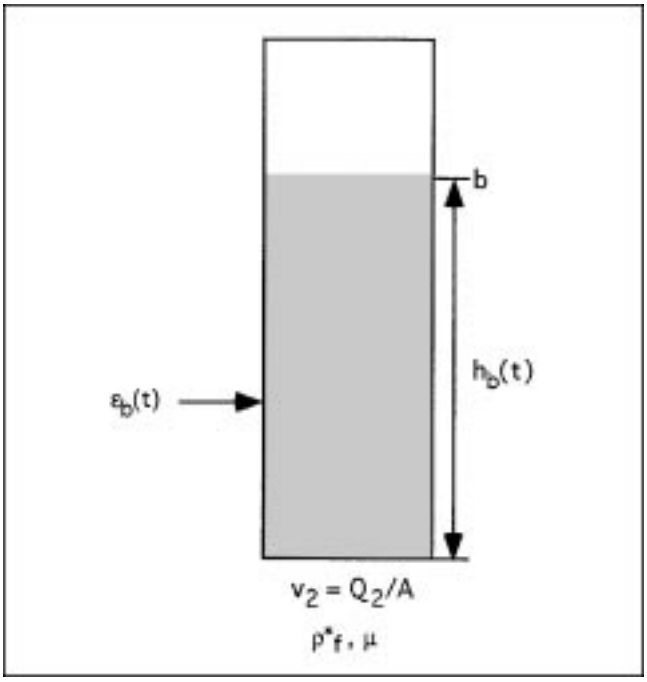

Figure 5. Idealized bed subjected to a step change in flow rate for the limit of infinite dispersion.

For a step increase in flow rate $h_1 < h_b(t)$ and $\epsilon_1 < \epsilon_b(t)$; for a step decrease in flow rate $h_1 > h_b(t)$ and $\epsilon_1 > \epsilon_b(t)$.

which upon simplification yields

$$\frac{dh_b}{dt} = v_{s,1}. \tag{51}$$

Substituting the particle velocity expression gives

$$\frac{dh_b}{dt} = v_2 - v_t(1-\phi_1)^n = v_2 - v_1. \tag{52}$$

The results (Eqs. 42 and 52) are exactly those obtained by Gibilaro et al. (1984). Equations 49 and 52 describe the transient state of the bed when subjected to a step change in the fluidization velocity for the limit of zero dispersion.

Infinite-Dispersion Limit. For the case of infinite dispersion, the bed is well mixed and no gradients in the solid fraction are assumed to exist. As such, the solid fraction is uniform throughout the bed and is proportional to the bed height. For this reason, the solid fraction can be determined from the particle-mass balance

$$\phi_b(t) = \frac{\phi_s h_s}{h_b(t)}. \tag{53}$$

Figure 5 shows the bed for the limit of infinite dispersion.

The mass flux across the b interface is zero

$$\phi_b\left(\frac{dh_b}{dt} - v_{s,b}\right) = 0. \tag{54}$$

Rearrangement of Eq. 54 yields the bed expansion rate

$$\frac{dh_b}{dt} = v_{s,b}, \tag{55}$$

where the particle velocity is

$$v_{s,b} = v_2 - v_t(1-\phi_b)^n. \tag{56}$$

Substitution of Eqs. 53 and 56 into Eq. 55 yields

$$\frac{dh_b}{dt} = v_2 - v_t\left(1 - \frac{\phi_s h_s}{h_b}\right)^n, \tag{57}$$

which is the governing equation for bed expansion due to a step change in flow rate for the limit of infinite dispersion.

Two-Phase Model. In actuality, the bed expansion is described by neither the zero-dispersion nor the finite-dispersion limits; however, these limits provide upper and lower bounds on the actual bed expansion characteristics. Inspection of the boundary conditions, Eqs. 34–35, shows that a change in the fluidization velocity affects the solid velocity, v_s, and hence this boundary disturbance propagates through the system, as governed by the model (Eqs. 33–39).

Discussion

A discussion of the model simulations and the experimental data for the expansion studies is now presented. Figures 6 and 7 show a comparison of simulations for all three models, as well as the experimental data. Figure 6 shows the results for five experimental runs where the volumetric flow rate was increased from 15 to 20, 25, 35, 45 and 55 mL/min. Figure 7 shows the results for four experimental runs where the volumetric flow rate was decreased from 45 to 15, 25, 35 and 40

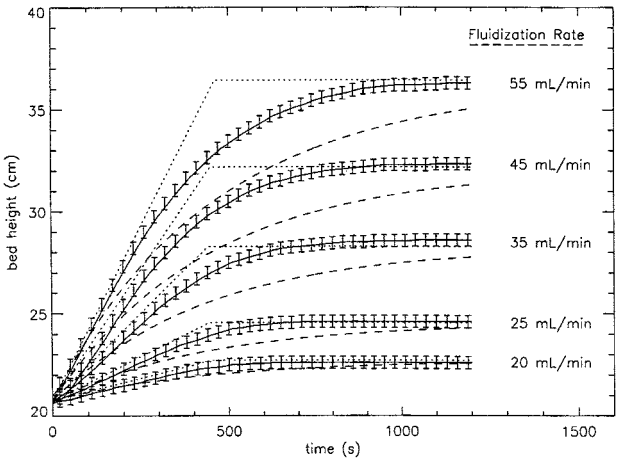

Figure 6. Dynamic response of bed height to a series of step increases in the fluidization velocity.

An initial fluidization velocity of 15 mL/min was used. *Key:* (····) Zero-dispersion limit; (– – –) infinite-dispersion limit; (——) two-phase model; and symbols are the experimental data with error bars of ±3 mm.

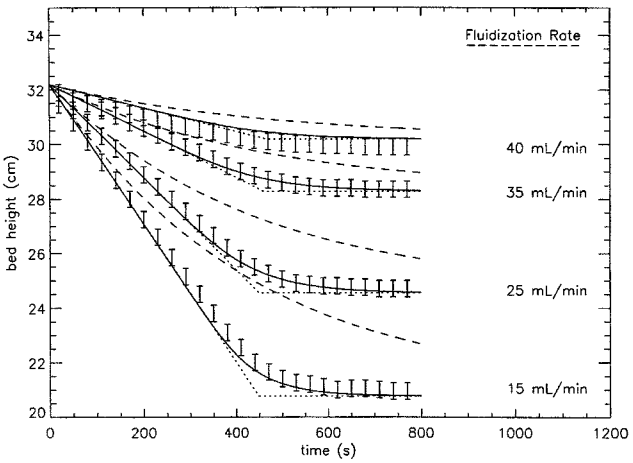

Figure 7. Dynamic response of bed height to a series of step decreases in the fluidization velocity.

An initial fluidization velocity of 45 mL/min was used. *Key:* (· · ·) zero-dispersion limit; (– – –) infinite-dispersion limit; (– – –) two-phase model; and symbols are the experimental data with error bars of ±3 mm.

mL/min. The experimental data with error bars of ±3 mm are also included in these plots. The zero-dispersion model closely follows the experimental data during the initial expansion period. However, after the bed has reached approximately 50% of its final height, the zero-dispersion model and the experimental data start to diverge. The zero-dispersion model shows a higher rate of change in the bed height than the experimental data and hence reaches the steady-state operating condition sooner. The infinite-dispersion model also closely follows the experimental data in the initial period after the step change. However, after the bed has reached approximately 20% of its final height, the infinite-dispersion model and the experimental data start to diverge. The infinite-dispersion model shows a much lower rate of change in the bed height than the experimental data, and hence reaches the steady-state operating condition at considerable time later than the experimental data. It is noted that the zero- and infinite-dispersion models bound the experimental bed expansion/contraction behavior, providing lower (infinite-dispersion model) and upper (zero-dispersion model) bounds. The two-phase model shows excellent agreement with the experimental data.

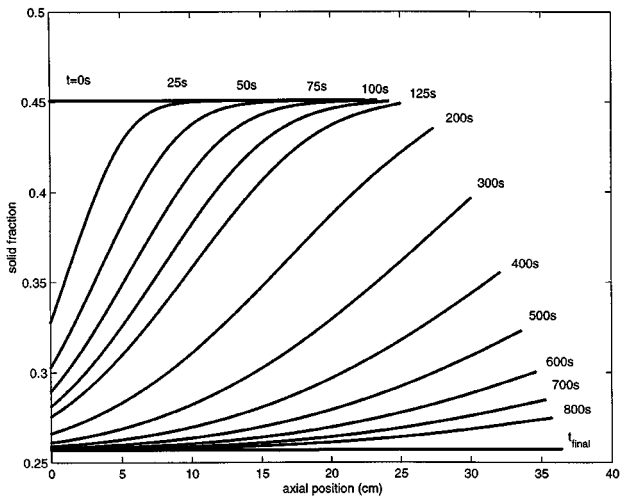

Figure 8. Solid fraction vs. axial position for a step change in the fluidization velocity from 15 to 55 mL/min.

Table 1. Dispersion-Coefficient Data for Flow-Rate Change Experiments

Fluidiz. Initial (cm/s)	Velocity Final (cm/s)	Dispers. Best Fit (cm^2/s)	Coefficient 10% Limits (cm^2/s)
0.0127	0.0170	0.08	0.06–0.12
0.0127	0.0212	0.10	0.07–0.16
0.0127	0.0297	0.18	0.13–0.23
0.0127	0.0382	0.20	0.16–0.24
0.0127	0.0467	0.37	0.34–0.40
0.0382	0.0127	0.05	0.02–0.08
0.0382	0.0212	0.07	0.04–0.16
0.0382	0.0297	0.08	0.04–0.16
0.0382	0.0339	0.14	0.05–0.26

Figure 8 shows the axial profile of the solid fraction at various times for a step increase in the fluidization velocity. The results indicate a smooth transition between the initial and final axial solid fraction profiles.

The solid-phase dispersion coefficient was treated as a free parameter and fitted by least-squares regression. Table 1 shows a listing of the solid-phase dispersion coefficients as obtained by least-squares fit along with bounds based upon sensitivity limits.

The values obtained for the solid-phase dispersion coefficient do correlate with the fluidization velocity, v_f. Figure 9 shows a log-log plot of solid-phase dispersion coefficient vs. the superficial velocity. The data fits a power law model

$$D_p = D(v_f)^{\alpha}, \tag{58}$$

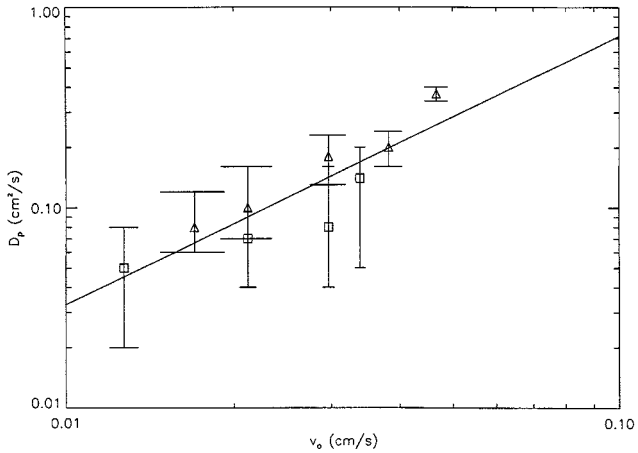

Figure 9. Log-log plot of dispersion coefficient vs. fluidization velocity ($\alpha = 1.34 \pm 0.62$, log $D = 1.20 \pm 1.0$, and $R^2 = 0.79$).

Key: □—step decrease in flow rate, and Δ—step increase in flow rate. Error bars represent ±10% sensitivity limits on the sum-squared error index.

with alpha equal to 1.34 and a correlation coefficient of 0.79. It is noted that various forms of the power-law model have been proposed for dispersion in porous media and solid–liquid flows (Ramirez et al., 1980; Dorgelo et al., 1985; Kang et al., 1990). An interesting observation is that the solid-phase dispersion coefficient does not appear to be strongly dependent upon whether a step increase or a step decrease in the fluidization velocity was implemented. The power-law model is a first attempt at correlating the solid-phase dispersion coefficient.

Fluid Property Changes

In this section, the following situation is considered. A bed of spherical particles of radius r_p and denity ρ_p^* is initially fluidized by a fluid of viscosity μ_1 and density ρ_1^* at a superficial velocity v_o. At steady state under these conditions, the solid fraction ϕ_1 is determined from

$$\frac{v_o}{v_{t,1}} = f_1(\phi_1), \tag{59}$$

where the terminal settling velocity of a single particle in the Stokes flow regime is

$$v_{t,1} = \frac{2r_p^2(\rho_p^* - \rho_1^*)g}{9\mu_1}. \tag{60}$$

The hindered settling function is given by the Richardson–Zaki expression

$$f_1(\phi_1) = (1-\phi_1)^n. \tag{61}$$

The steady-state height of the bed under these conditions is determined from a particle-mass balance

$$h_1 = \frac{\phi_s h_s}{\phi_1}, \tag{62}$$

where ϕ_s and h_s are the solid fraction and height of the settled bed, respectively, before fluidization.

Now, suppose that the fluid entering the bottom of the bed experiences a step change in fluid properties (viscosity and/or density) at $t = 0$, so that the bed adjusts to a new steady state given by Eqs. 59–62, but with the subscript 2 (for the new fluid properties) replacing 1. The question to be addressed is how the transient occurs as the bed moves to the new steady state. The simplified two-phase model (Eqs. 33–39) is applied in order to address this question. The simplified model based upon the assumption of zero dispersion is also presented. A model for the limit of infinite dispersion cannot be derived in a simple form.

Experimental system

A STREAMLINE 50 column (5 cm ID) was used in the fluidization studies with STREAMLINE SP adsorbent. The resin has a mean diameter of 186 μm and a mean density of 1.184 g/cm^3 (Chang and Chase, 1996). The column and required ancillary equipment are shown in Figure 1. Feedstock was delivered to the column by means of a computer-controlled peristaltic pump (Cole-Parmer). The system was configured so as to allow on-line computer-controlled switching of feed stock between two supply tanks.

Table 2. Physical Property Data for Feed-Stock Solutions Used in the Fluid-Property Experiments

Feedstock	Dens. g/cm^3	95% CI g/cm^3	Vis. cp	95% CI cp	Particle *Re* No.	Modified Re. No.
Water	0.9972	—	0.890	—	0.82	0.065–0.14
Glycerol 1	1.026	0.00017	1.129	0.0142	0.45	0.049–0.10
Glycerol 2	1.040	0.00013	1.337	0.0060	0.29	0.041–0.086
Glycerol 3	1.054	0.00017	1.572	0.0140	0.19	0.033–0.069
Dextran 1	1.004	0.00017	1.162	0.0075	0.47	0.049–0.10
Dextran 2	1.006	0.00007	1.347	0.0109	0.35	0.039–0.082
Dextran 3	1.007	0.00011	1.583	0.0112	0.25	0.032–0.066

Three feed stocks were utilized in the experiments in order to determine the bed-expansion characteristics for step changes in fluid properties. In all studies, the bed was initially fluidized with deionized (DI) water. Step changes were then made to either aqueous glycerol solutions or aqueous dextran solutions at varying concentrations. Aqueous dextran (Pharmacia Biotech) solutions were made at three different concentrations. As the solutions were rather dilute, viscosity could be adjusted almost independent of density. Likewise, three aqueous glycerol (Fischer) solutions were prepared at the same viscosities as the dextran solutions. The density of the glycerol solution varied significantly. Table 2 shows physical properties at 25°C for the solutions along with confidence intervals (CI). The confidence intervals were evaluated from triplicate experimental runs and root-mean square propagation of error analysis.

The bed was fluidized with each of the feed stocks listed in Table 2. The bed was considered to be in a stable state of fluidization if channeling was observed to be minimal in the lower region of the column. A linear regression was performed for log-log plots of the superficial fluidization velocity versus the void fraction. Table 3 summarizes the experimentally determined Richardson–Zaki parameters. The theoretically calculated Stokes velocities are also listed. The regressed and theoretical Stokes values agree within experimental uncertainty for all feed stocks. The error bounds for the theoretical values are broad, due in large part to the inability to accurately determine the mean particle diameter.

Table 3. Richardson–Zaki Parameters for Feed-Stock Solutions Used in the Fluid-Property Experiments

Feedstock	n Regress.	95% CI	V_t Regress. cm/s	95% CI cm/s	V_t Theor. cm/s	95% CI cm/s
Water	5.19	5.01–5.37	0.374	0.342–0.408	0.395	±0.073
Glycerol 1	5.15	4.90–5.40	0.269	0.241–0.300	0.264	0.052
Glycerol 2	5.17	5.00–5.34	0.240	0.224–0.258	0.202	0.042
Glycerol 3	4.88	4.64–5.13	0.173	0.158–0.189	0.155	0.034
Dextran 1	5.52	5.16–5.88	0.353	0.299–0.417	0.292	0.055
Dextran 2	4.96	4.73–5.20	0.229	0.207–0.253	0.249	0.047
Dextran 3	4.55	4.29–4.80	0.169	0.153–0.188	0.211	0.040

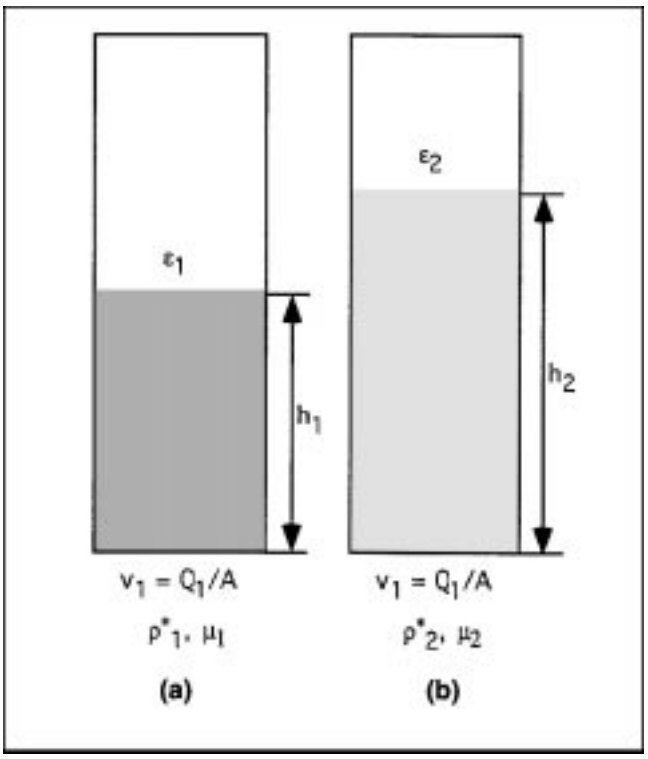

Figure 10. Fluidized bed before (a) and after (b) a fluid property change ($\epsilon_1 < \epsilon_2$).

The Richardson–Zaki exponent varied considerably, ranging from 4.55 to 5.52. Both the Reynolds number and the modified Reynolds number for the feed stock solutions are well within the Stokes flow regime. The two values listed in Table 2 for the modified Reynolds number are for fluidization rates of 20 and 50 mL/min.

Models for fluid property change

In this section, two models are presented to address the question of how the transient occurs as the bed moves to a new steady state for a step change in fluid properties. The first model is based upon the limiting condition of zero dispersion, and the second model is the two-phase model (Eqs. 33–39).

Zero-Dispersion Limit. We consider the case where the bed expands (i.e., $\phi_2 < \phi_1$ or $v_{t,1} < v_{t,2}$). Figure 10 shows a schematic representation of the steady-state conditions both before and after the step change in fluid properties. As the front separating the two fluids (plug flow of the fluid is assumed) first enters the bed, the particles near the bottom of the bed will be lifted upwards because their lower settling velocity in the new fluid no longer balances the upward superficial velocity of fluidization, that is

$$v_{t,2} f_1(\phi_1) < v_o = v_{t,1} f_1(\phi_1). \tag{63}$$

If the bed were to simply rise as a plug, with the void fraction remaining at ϵ_1, this would create a growing layer of clear fluid beneath the rising plug. However, a concentrated region of particles above clear fluid is unstable, and so we expect that particles fall away from the bottom of the rising concentrated region into the less concentrated region below (unless there are strong cohesive forces between the particles which hold the plug together). It is expected that the growing lower region near the bottom of the bed is at a void fraction of ϵ_2, so that the particles on average are stationary in this region due to a balance of buoyancy and drag forces. Just above the rising front of new fluid, the particles are not stationary but rather move upwards because their hindered settling velocity in fluid 1 is less than the superficial velocity. In an effect similar to that experienced by snow in front of a plow, these rising particles collide with the stationary particles above and accumulate in a growing band of concentrated particles with a void fraction ϵ_c. Above the concentrated band, the particles will be at the original void fraction ϵ_1 in the original fluid 1, and hence remain stationary until the top of the concentrated band reaches the height of the original bed h_1. Figure 11 shows this process. In Figure 11, $h_b(t)$ is the bed height, $h_i(t)$ is the height of the interface between fluids 1 and 2, and $h_c(t)$ is the height of the interface between the compacted zone and the undisturbed zone.

The velocities of the interfaces dh_i/dt, dh_c/dt, and dh_b/dt can be determined from mass balances. The velocity of the i interface is equal to the fluid velocity

$$\frac{dh_i}{dt} = v_f, \tag{64}$$

which upon substitution of Eq. 85 yields

$$\frac{dh_i}{dt} = \frac{v_o}{\epsilon_2} - \frac{\phi_2}{\epsilon_2} v_{s,2,2}. \tag{65}$$

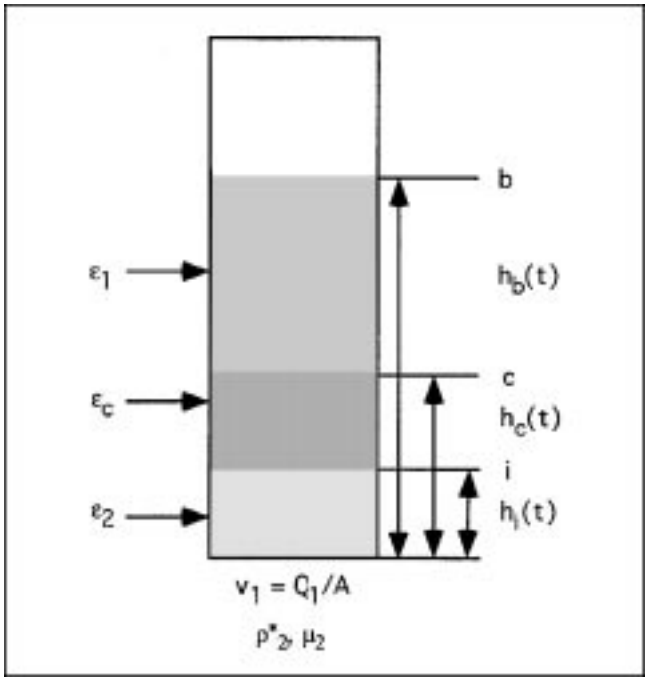

Figure 11. Fluidized bed subjected to a step change in fluid properties for the limit of zero dispersion ($\epsilon_c < \epsilon_1 < \epsilon_2$).

The solids velocity $v_{s,2,2}$ {the subscripts on $v_{s,\alpha,\beta}$ have the following meaning: s indicates the solid; α indicates the fluid properties; and β indicates the local void fraction [$v_{s,\alpha,\beta} = v_o - v_{t,\alpha}(1-\phi_\beta)^n$]} is zero, so that

$$\frac{dh_i}{dt} = \frac{v_o}{\epsilon_2}. \tag{66}$$

Now, across the i interface, the mass flux of solid entering is equal to the mass flux of solid leaving

$$\phi_2\left(\frac{dh_i}{dt} - v_{s,2,2}\right) = \phi_c\left(\frac{dh_i}{dt} - v_{s,1,c}\right). \tag{67}$$

Equation 67 can be rearranged in terms of the particle velocity in the compacted zone

$$v_{s,1,c} = \frac{\phi_c - \phi_2}{\phi_c}\frac{dh_i}{dt}. \tag{68}$$

Substituting for the particles velocity $v_{s,1,c}$ yields

$$v_o - v_{t,1}(1-\phi_c)^n = \frac{\phi_c - \phi_2}{\phi_c}\frac{dh_i}{dt}, \tag{69}$$

which is further simplified by substitution of Eq. 66 for the i interface velocity dh_i/dt

$$v_o - v_{t,1}(1-\phi_c)^n = \frac{\phi_c - \phi_2}{\phi_c}\frac{v_o}{\epsilon_2}. \tag{70}$$

Equation 70 can be solved for ϕ_c. Likewise, across the c interface, the mass flux of solid entering is equal to the mass flux of solid leaving

$$\phi_c\left(\frac{dh_c}{dt} - v_{s,1,c}\right) = \phi_1\left(\frac{dh_c}{dt} - v_{s,1,1}\right). \tag{71}$$

Noting that the particle velocity $v_{s,1,1}$ is equal to zero, the following expression for the c interface velocity is obtained

$$\frac{dh_c}{dt} = \frac{\phi_c}{\phi_c - \phi_1}v_{s,1,c}. \tag{72}$$

Also, across the b interface, the mass flux of solid entering is equal to the mass flux of solid leaving

$$\phi_1\left(\frac{dh_b}{dt} - v_{s,1,1}\right) = 0, \tag{73}$$

which upon simplification yields

$$\frac{dh_b}{dt} = 0. \tag{74}$$

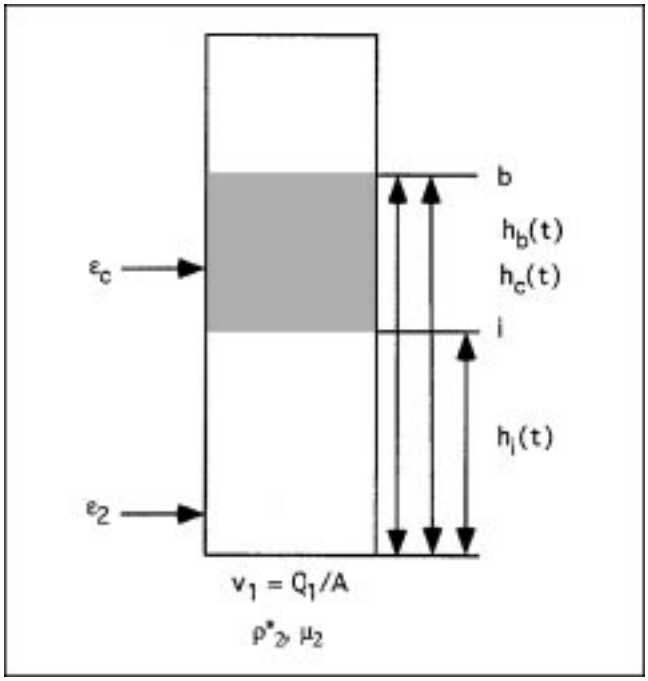

Figure 12. Fluidized bed subjected to a step change in fluid properties for the limit of zero dispersion; compacted zone has just reached the top of the bed.

The bed will remain stationary until the top of the concentrated band reaches the top of the bed. Figure 12 shows the void fraction profile at the time when the bed just begins to move. Now, the mass-balance condition across the b interface is given by

$$\phi_c\left(\frac{dh_b}{dt} - v_{s,1,c}\right) = 0, \tag{75}$$

which results in the following equation for the bed expansion rate

$$\frac{dh_b}{dt} = v_{s,1,c} = v_o - v_{t,1}(1-\phi_c)^n. \tag{76}$$

Two-Phase Model. In actuality, the bed expansion is only approximated by the zero-dispersion model. Inspection of the boundary conditions, Eqs. 34–35, shows that a change in the fluidization properties affects the solid velocity, v_s, and hence this boundary disturbance propagates through the system, as governed by the model (Eqs. 33–39).

Discussion

A series of experiments were performed in order to determine the bed expansion properties for a step change in the fluid properties. In these experiments, the bed was initially fluidized with DI water at a given flow rate. Upon reaching a state of uniform fluidization, as indicated by a constant degree of expansion, a step change was made to a fluid with

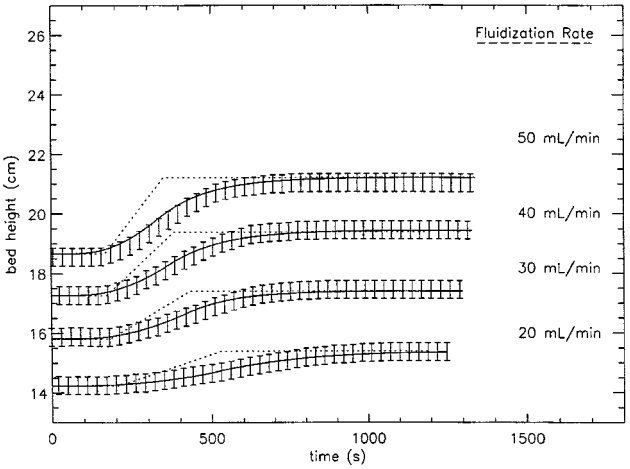

Figure 13. Transient bed-height expansion experiment for a step change in fluid properties.

Step change from DI water to glycerol 1 solution. *Key:* (——) two-phase model; (· · ·) zero-dispersion model; symbols are experimental data with error bars of ±3 mm.

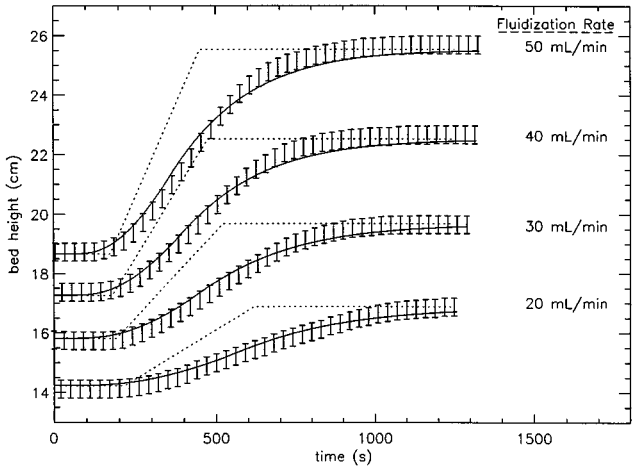

Figure 15. Transient bed-height expansion experiment for a step change in fluid properties.

Step change from DI water to glycerol 3 solution. *Key:* (——) two-phase model; (· · ·) zero-dispersion model; symbols are experimental data with error bars of ±3 mm.

different physical properties. Two fluids were investigated in this study. Aqueous glycerol solutions were prepared that allowed the density and viscosity of the solution to be varied. Aqueous dextran solutions were also prepared that allowed the independent manipulation of the viscosity.

After the introduction of the step change, the bed height was recorded as a function of time. Figures 13–18 show plots of the bed height vs. time for the experimental runs. The solid lines are the two-phase model, the dashed lines are the zero-dispersion model, and the symbols are the experimental values, including error bounds of ±3 mm. A comparison of Figures 13–18 shows that the zero-dispersion model predicts a much higher bed expansion rate than observed experimentally, while the two-phase model shows excellent agreement with the experimental data. In Figures 13–18, the time delay in bed expansion for both the models agree well with the experimental data. The time delay is a result of the compacting zone, as depicted in Figures 11 and 12. The compacted zone takes a finite amount of time to reach the top of the bed, at which point the bed begins to expand. Figure 19 shows a plot of the solid fraction vs. the axial position for a number of time slices. The simulation results depict how the compacted zone looks when the dispersion effects are considered. In comparing Figures 8 and 19, it is clearly evident that changes in fluidization velocity do not create a compacted zone within the bed, as was observed for the fluid property changes. The compacted zone is the reason for the observed time delay associated with step changes in fluid properties.

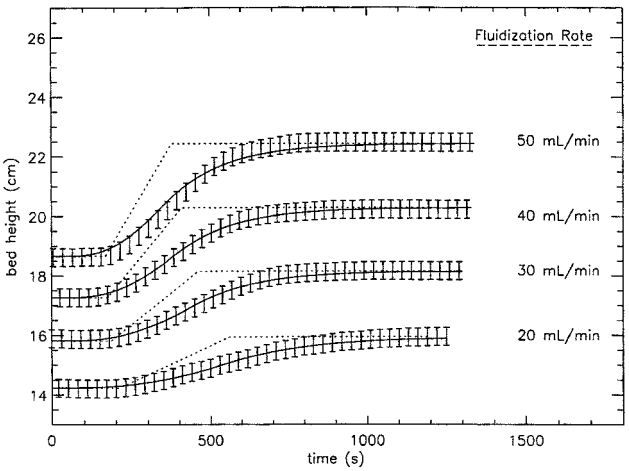

Figure 14. Transient bed-height expansion experiment for a step change in fluid properties.

Step change from DI water to glycerol 2 solution. *Key:* (——) two-phase model; (· · ·) zero-dispersion model; symbols are experimental data with error bars of ±3 mm.

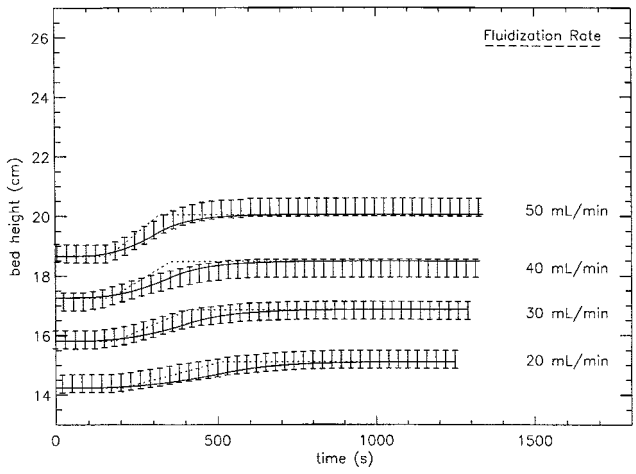

Figure 16. Transient bed-height expansion experiment for a step change in fluid properties.

Step change from DI water to dextran 1 solution. *Key:* (——) two-phase model; (· · ·) zero-dispersion model; symbols are experimental data with error bars of ±3 mm.

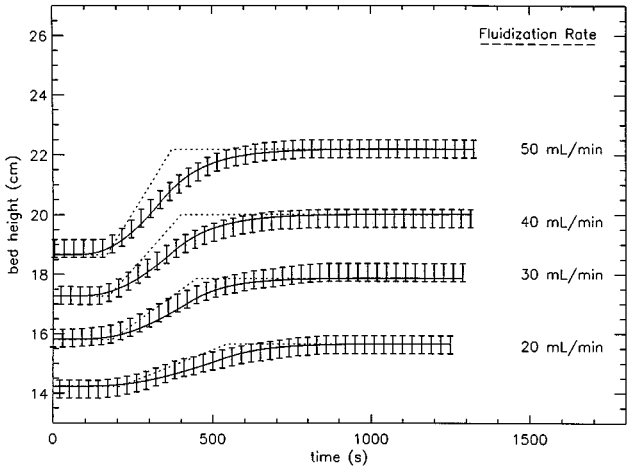

Figure 17. Transient bed-height expansion experiment for a step change in fluid properties.

Step change from DI water to dextran 2 solution. *Key:* (——) two-phase model; (· · ·) zero-dispersion model; symbols are experimental data with error bars of ±3 mm.

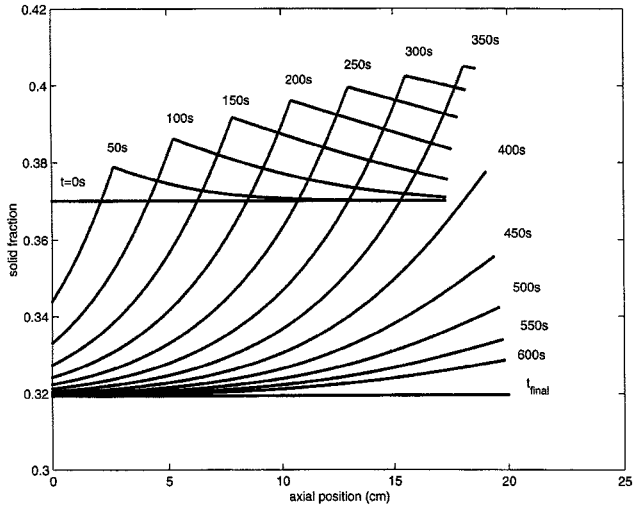

Figure 19. Solid fraction vs. axial position for a step change from water to the dextran 2 solution at 40 mL/min.

The solid-phase dispersion coefficient was treated as a free parameter and fitted by least-squares regression. Table 4 shows a listing of the solid-phase dispersion coefficients as obtained by least-squares fit, while Figure 20 shows a log-log plot of the solid-phase dispersion coefficient vs. the fluidization velocity. The solid-phase dispersion coefficient is statistically independent of the fluidization velocity for the glycerol data with *F*-values well above the testing level of 0.05 (Table 5). The solid-phase dispersion coefficient shows a definite decrease from the glycerol-1 to the glycerol-3 solutions. For the dextran-1 data, the solid-phase dispersion coefficient shows no velocity dependence, while the dextran-2 data show a dependence on velocity. The dextran-3 data have an *F*-value of 0.06, which is in the interval of usual testing levels of 0.05 to 0.1; therefore, the solid-phase dispersion coefficient correlates with velocity with marginal certainty. Again, the dextran data show a decrease in the solid-phase dispersion coefficient with an increase in fluid viscosity and density, as do the glycerol data. Table 5 summarizes the statistical properties of the power-law model with alpha equal to zero and a regressed alpha.

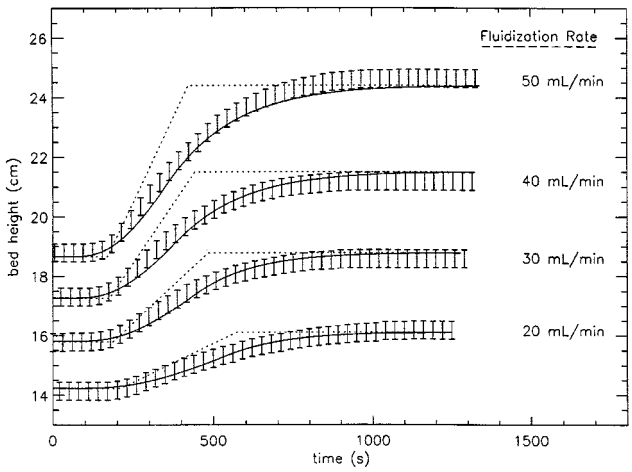

Figure 18. Transient bed-height expansion experiment for a step change in fluid properties.

Step change from DI water to dextran 3 solution. *Key:* (——) two-phase model; (· · ·) zero-dispersion model; symbols are experimental data with error bars of ±3 mm.

Table 4. Dispersion-Coefficient Data for Fluid-Property-Change Experiments

Feedstock	Fluidiz. Velocity (cm/s)	Dispers. Best fit (cm^2/s)	Coeff. 10% Limits (cm^2/s)
Glycerol 1	0.0170	0.86	0.78–0.98
Glycerol 1	0.0255	0.55	0.52–0.58
Glycerol 1	0.0340	0.73	0.64–0.78
Glycerol 1	0.0425	0.82	0.70–0.90
Glycerol 2	0.0170	0.63	0.58–0.67
Glycerol 2	0.0255	0.55	0.48–0.63
Glycerol 2	0.0340	0.60	0.50–0.70
Glycerol 2	0.0425	0.68	0.54–0.76
Glycerol 3	0.0170	0.52	0.43–0.64
Glycerol 3	0.0255	0.50	0.44–0.57
Glycerol 3	0.0340	0.53	0.44–0.60
Glycerol 3	0.0425	0.51	0.45–0.56
Dextran 1	0.0170	0.36	0.28–0.45
Dextran 1	0.0255	0.36	0.30–0.46
Dextran 1	0.0340	0.66	0.50–0.80
Dextran 1	0.0425	0.41	0.38–0.47
Dextran 2	0.0170	0.19	0.15–0.25
Dextran 2	0.0255	0.27	0.22–0.36
Dextran 2	0.0340	0.36	0.30–0.44
Dextran 2	0.0425	0.45	0.41–0.47
Dextran 3	0.0170	0.22	0.18–0.28
Dextran 3	0.0255	0.24	0.18–0.35
Dextran 3	0.0340	0.31	0.26–0.40
Dextran 3	0.0425	0.42	0.35–0.46

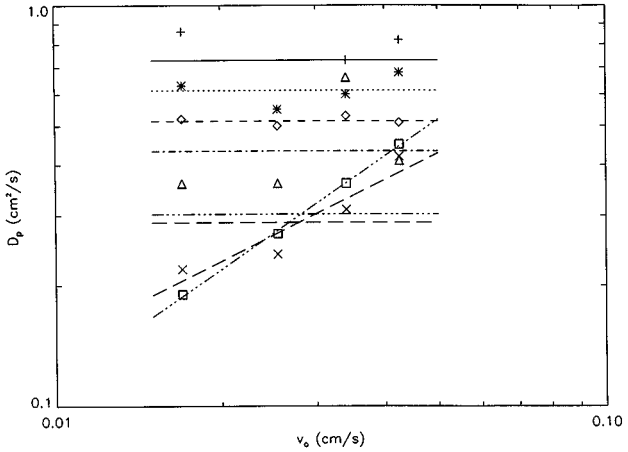

Figure 20. Log-log plot of the dispersion coefficient vs. fluidization velocity.

Key: (+, ——) glycerol 1; (∗, · · ·) glycerol 2; (◇, – – –) glycerol 3; (Δ, –·) dextran 1; (□, –· · ·) dextran 2; and (X, — —) dextran 3.

An interesting finding is that as the magnitude of the viscosity and/or density change increases, the dependence of the solid-phase dispersion coefficient on the velocity is weaker. However, more research needs to be performed in order to determine a precise correlation of the solid-phase dispersion coefficient with the fluid density, viscosity, and fluid velocity.

Conclusions

In this article, two-phase theory has been applied to solid–liquid fluidization in the Stokes flow regime. Since the inertial terms can be neglected in the Stokes flow regime, the linear momentum balances are simplified to algebraic constraints. The simplified linear momemtum balance considered three forces, namely, drag, buoyant, and diffusive. The force-balance expression was then combined with the continuity equations, to obtain a governing equation for solid–liquid fluidization in the Stokes regime. This simplified two-phase equation was then applied to an experimental EBA system. Two flows were investigated, namely, step changes in the fluidization velocity and step changes in the fluid properties. Experimental data and model simulations were in excellent agreement for both flow configurations. Furthermore, the two-phase model provided an accurate prediction of the observed time delay in bed expansion for step changes in fluid properties, as well as a mechanistic explanation for its observation.

Table 5. Error Analysis of Dispersion-Coefficient Data for Fluid-Property-Change Experiments

Feedstock	α	SE 95%	log D (cm^2/s)	SE 95%	Statist. Signif. F-value
Glycerol 1	−0.01	±1.54	−0.15	±2.40	0.97
Glycerol 2	−0.08	±0.64	−0.09	±1.00	0.66
Glycerol 3	−0.001	±0.19	−0.29	±0.30	0.98
Dextran 1	0.36	±1.93	0.19	±3.00	0.51
Dextran 2	0.94	±0.11	0.94	±0.17	0.00073
Dextran 3	0.69	±0.78	0.53	±1.22	0.063
Feedstock	α	SE 95%	D_p (cm^2/s)	SE 95%	
Glycerol 1	0	—	0.74	±0.14	0.97
Glycerol 2	0	—	0.62	±0.05	0.66
Glycerol 3	0	—	0.52	±0.01	0.98
Dextran 1	0	—	0.45	±0.14	0.51
Dextran 2	0	—	0.32	±0.11	0.00073
Dextran 3	0	—	0.30	±0.09	0.063

Acknowledgments

The authors thank the following organizations for financial support: Pharmacia Biotech, The Colorado Institute for Research in Biotechnology, The National Institutes of Health, and the Whitaker Foundation. Professors V. H. Barocas and R. H. Davis of the University of Colorado, Department of Chemical Engineering, are gratefully acknowledged for their stimulating conversations with the authors regarding the subject of this article. Both Professors Barocas and Davis contributed ideas to the simplified mass-balance approach of modeling.

Notation

A = cross-sectional area of column
D_p = particle-phase dispersion coefficient
h = bed height
m = mass of a single particle
Q_1 = liquid volumetric flow rate before step change
Q_2 = liquid volumetric flow rate after step change
t = time
z = axial position
β_1 = drag parameter
β_2 = dispersion parameter
ϕ_2 = solid fraction after step change
μ_2 = viscosity after step change
ρ_2^* = fluid density after step change
ρ_s = solid-phase density
τ = relaxation parameter

Literature Cited

Asif, M., J. N. Petersen, E. N. Kaufman, J. M. Cosgrove, and T. C. Scott, "A Dynamic Model of the Hydrodynamics of a Liquid Fluidized Bed," *Ind. Eng. Chem. Res.*, **33**, 2151 (1994).

Barnea, E., and J. Mizrahi, "A Generalized Approach to the Fluid Dynamics of Particulate Systems: Part 1, General Correlation for Fluidization and Sedimentation in Solid Multiparticle Systems," *Chem. Eng. J.*, **5**, 171 (1973).

Barthels, C. R., G. Kleiman, J. N. Korzun, and D. B. Irish, "A Novel Ion-Exchange Method for the Isolation of Streptomycin," *Chem. Eng. Prog.*, **54**, 49 (1958).

Batt, B. C., V. M. Yabannavar, and V. Singh, "Expanded Bed Adsorption Process for Protein Recovery from Whole Mammalian Cell Culture Broth," *Bioseparation*, **5**, 41 (1995).

Bedford, A., and D. S. Drumheller, "Theories of Immiscible and Structured Mixtures," *Int. J. Eng. Sci.*, **21**(8), 863 (1983).

Chang, Y. K., and H. A. Chase, "Development of Operating Conditions for Protein Purification Using Expanded Bed Techniques: The Effect of the Degree of Bed Expansion on Adsorption Performance," *Biotechnol. Bioeng.*, **49**, 512 (1996).

Chase, H. A., and N. M. Draeger, "Affinity Purification of Proteins Using Expanded Beds," *J. Chromatogr.*, **597**, 129 (1992a).

Chase, H. A., and N. M. Draeger, "Expanded-Bed Adsorption of Proteins Using Ion-Exchange," *Sep. Sci. Technol.*, **27**, 2021 (1992b).

Coulson, J. M., J. F. Richardson, J. R. Backhurst, and J. H. Harker, *Chemical Engineering: Particle Technology and Separation Processes*, 4th ed., Pergamon Press, Oxford (1991).

Crank, J., *Free and Moving Boundary Problems*, Clarendon Press, Oxford (1984).

Dasari, G., "High-Performance Liquid Chromatography of Amino Acids, Peptides, and Proteins," *J. Chromatogr.*, **631**, 115 (1993).
Davis, R. H., "Velocity of Sedimenting Particles in Suspensions," *Sedimentation of Small Particles in a Viscous Fluid*, E. M. Tory, ed., Computational Mechanics Publications, South Hampton, UK (1995).
Davis, R. H., and K. H. Birdsell, "Hindered Settling of Semidilute Monodisperse and Polydisperse Suspensions," *AIChE J.*, **34**(1), 123 (1988).
DeLuca, L., D. Hellenbroich, N. J. Titchener-Hooker, and H. A. Chase, "A Study of the Expansion Characteristics and Transient Behavior of Expanded Beds of Adsorbent Particles Suitable for Bioseparations," *Bioseparation*, **4**, 311 (1994).
Dorgelo, E. A. H., A. P. Van Der Meer, and J. A. Wesselingh, "Measurement of the Axial Dispersion of Particles in a Liquid Fluidized Bed Applying Random Walk Model," *Chem. Eng. Sci.*, **42**, 2333 (1985).
Draeger, N. M., "The Use of Fluidized Beds for the Purification of Proteins," PhD Thesis, Univ. of Cambridge, Cambridge, England (1991).
Draeger, N. M., and H. A. Chase, *Trans. Inst. Chem. Eng., C*, **69**, 45 (1991).
Fan, L.-T., J. A. Schmitz, and E. N. Miller, "Dynamics of Liquid-Solid Fluidization Bed Expansion," *AIChE J.*, **9**(2), 149 (1963).
Gailliot, F. P., C. Gleason, J. J. Wilson, and J. Zwarick, "Fluidized Bed Adsorption for Whole Broth Extraction," *Biotechnol. Prog.*, **6**, 370 (1990).
Garside, J., and M. R. Al-Dibouni, "Velocity-Voidage Relationships for Fluidization and Sedimentation in Solid-Liquid Systems," *Ind. Eng. Chem. Process Des. Dev.*, **16**, 206 (1977).
Gibilaro, L. G., S. P. Waldram, and P. U. Foscolo, "A Simple Mechanistic Description of the Unsteady State Expansion of Liquid Fluidized Beds," *Chem. Eng. Sci.*, **39**(3), 610 (1984).
Green, A. E., and P. M. Naghdi, "On Basic Equations for Mixtures," *Q. J. Mech. Appl. Math.*, **22**(4), 427 (1969).
Hansson, M., J. Stahl, R. Hjorth, M. Uhlen, and T. Moks, "Single-Step Recovery of a Secreted Recombinant Protein by Expanded-Bed Adsorption," *Bio/Technology*, **12**, 285 (1994).
Hinze, J. O., "Momentum and Mechanical-Energy Balance Equations for a Flowing Homogeneous Suspension with Slip Between the Two Phases," *Appl. Sci. Res.*, Sec. A, **11**(1), 33 (1962).
Kang, Y., J. B. Nah, B. T. Min, and S. D. Kim, "Dispersion and Fluctuation of Fluidized Particles in a Liquid-Solid Fluidized Bed," *Chem. Eng. Commun.*, **97**, 197 (1990).
Kennedy, S. C., and R. H. Bretton, "Axial Dispersion of Spheres Fluidized with Liquids," *AIChE J.*, **12**(1), 24 (1966).
Kenyon, D. E., "The Theory of an Incompressible Solid-Fluid Mixture," *Arch. Rat. Mech. Anal.*, **62**, 131 (1976).
Lamb, H., *Hydrodynamics*, 6th ed., Cambridge Univ. Press (1932).
Landau, H. G., *Q. Appl. Math.*, **8**, 81 (1950).
Müller, I., "A Thermodynamic Theory of Mixtures of Fluids," *Arch. Rat. Mech. Anal.*, **28**(1), 1 (1968).
Peddieson, J., Jr., "On Continuum Description of Solid-Fluid Suspensions," *Dev. Theor. Appl. Mech.*, **7**, 355 (1974).
Poncelet, D., H. Naveau, E.-D. Nyns, and D. Dochain, "Transient Response of a Solid-Liquid Model Biological Fluidized Bed to a Step Change in Fluid Superficial Velocity," *J. Chem. Tech. Biotechnol.*, **48**, 439 (1990).
Ramirez, W. F., P. J. Shuler, and F. Friedman, "Convection, Dispersion, and Adsorption of Surfactants in Porous Media," *Soc. Pet. Eng. J.*, 430 (1980).
Richardson, J. F., and W. N. Zaki, "Sedimentation and Fluidization: Part I," *Trans. Inst. Chem. Eng.*, **32**, 35 (1954).
Slis, P. L., T. Willemse, and H. Kramers, "The Response of the Level of a Liquid Fluidized Bed to a Sudden Change in the Fluidizing Velocity," *Appl. Sci. Res.*, **8**, 209 (1959).
Somers, W., K. van't Reit, H. Rozie, F. M. Rombouts, and J. Visser, "Isolation and Purification of Endo-Polygalacturonase by Affinity Chromatography in a Fluidized-Bed Reactor," *Chem. Eng. J.*, **40**, B7 (1989).
Soo, S. L., "Pipe Flow of Suspensions," *Appl. Sci. Res.*, **21**, 68 (1969).
Stokes, G. G., *Mathematical and Physical Papers*, (1901).
Thelen, T. V., and W. F. Ramirez, "Bed-Height Dynamics of Expanded Beds," *Chem. Eng. Sci.*, **52**(19), 3333 (1997).
Truesdell, C., "Mechanical Basis of Diffusion," *J. Chem. Phys.*, **37**(10), 2336 (1962).
van Deemter, J. J., and E. T. van der Laan, "Momentum and Energy Balances for Dispersed Two-Phase Flow," *Appl. Sci. Res.*, Sec. A, **10**(2), 102 (1961).
Zuber, N., "On the Dispersed Two-Phase Flow in the Laminar Flow Regime," *Chem. Eng. Sci.*, **19**, 897 (1964).

Appendix A

Here, we derive the particle-velocity expression. Consider the case where solid-phase dispersion forces are negligible. The drag and buoyant forces are balanced, and Eq. 21 is applicable, which is written as

$$\frac{v_r}{v_t} = \frac{v_f - v_p}{v_t} = (1-\phi)^{n-1}. \tag{A1}$$

Here it has been assumed that the hindered settling function is given by the Richardson–Zaki correlation. Substitution of Eq. 38 into Eq. A1 yields

$$\frac{\dfrac{v_o}{\epsilon} - \dfrac{\phi}{\epsilon} v_p - v_p}{v_t} = (1-\phi)^{n-1}. \tag{A2}$$

After rearranging Eq. A2 is expressed as

$$v_p = v_o - v_t(1-\phi)^n, \tag{A3}$$

where the Stokes settling velocity is calculated based upon local fluid properties.

Appendix B

Now, the continuity equations are utilized in order to obtain a relationship between the fluid velocity, v_f, and the particle velocity, v_p. Adding the liquid-phase and solid-phase continuity equations yields

$$\frac{\partial \epsilon}{\partial t} + \frac{\partial \phi}{\partial t} = -\frac{\partial(\epsilon v_f)}{\partial z} - \frac{\partial(\phi v_p)}{\partial z}, \tag{B1}$$

which is simplified as

$$\frac{\partial(\epsilon v_f)}{\partial z} + \frac{\partial(\phi v_p)}{\partial z} = 0, \tag{B2}$$

noting that

$$\frac{\partial \epsilon}{\partial t} + \frac{\partial \phi}{\partial t} = \frac{\partial(\epsilon + \phi)}{\partial t} = 0. \tag{B3}$$

Integrating Eq. B2 yields

$$\epsilon v_f + \phi v_p = k, \tag{B4}$$

where k is a constant of integration. It is known when $v_p = 0$, that $v_f = v_o/\epsilon$, thus allowing evaluation of the constant, which

yields

$$\epsilon v_f + \phi v_p = v_o. \tag{B5}$$

Rearranging Eq. B5 in terms of the fluid velocity gives

$$v_f = \frac{v_o}{\epsilon} - \frac{\phi}{\epsilon} v_p = \frac{v_o}{1-\phi} - \frac{\phi}{1-\phi} v_p. \tag{B6}$$

Equation B6 is a consequence of the conservation of mass and clearly shows that in general

$$v_f \neq \frac{v_o}{\epsilon}. \tag{B7}$$

A failure to appreciate this result is an oversight often encountered in the literature, where most authors incorrectly conclude that

$$v_f = \frac{v_o}{\epsilon} \tag{B8}$$

is always valid. The analysis here clearly shows that the condition (Eq. B8) is correct only under the limiting conditions, $v_p \to 0$ or $\phi \to 0$.

Manuscript received July 14, 1998.